Sol-gel synthesis of 13-93 bioactive glass powders containing therapeutic agents

Aylin M. Deliormanlı* and Mehmet Yıldırım

Celal Bayar University, Department of Materials Engineering, Manisa, Turkey

Email: aylin.deliormanli@cbu.edu.tr, aylin.deliormanli12@gmail.com

Available online at: www.austceram.com/ACS-Journal

Abstract
In the current study cerium or gallium- containing silicate based 13-93 bioactive glass powders were prepared using sol-gel method. Cerium and gallium ions were chosen due to their well-known therapeutic actions and antimicrobial properties. Effect of cerium and gallium substitution (up to 5w%) on the in vitro bioactivity, and mechanical properties of the prepared powders and scaffolds were assessed. Results revealed that, additions of cerium or gallium has no significant negative effect for in vitro bioactivity and hydroxyapatite forming ability of the glass for long immersion times in simulated body fluid. An increase in mechanical properties was observed in cerium doped (>3%) glass samples presumably due to CeO_2 formation during sintering. It was concluded that bioactive glass powders containing therapeutic metal ions prepared in the study via sol-gel process may find applications in biomedical applications in near future.

Keywords: Bioactive glass; sol-gel; powders; biomedical applications.

1. Introduction

Bioactive glass has recently become one of the most promising biomaterials for tissue engineering applications. These materials are able to induce specific biological activity when they exposed to aqueous environment. The bioactivity is achieved with the formation on their surfaces of a hydroxyapatite (HA)-layer, which bonds strongly to both hard and soft tissues and releases ion products after dissolution [1-3].

Bioactive glasses can be formed using melt-cast or sol-gel methods [1,3-5]. In the traditional melt-quenching route generally temperatures above 1100-1300°C is applied to melt the oxides together in a platinum crucible, while graphite molds (for monoliths), water or cold stain steel plates (for frit production) are used for quenching. Sol-gel method offers an alternative to traditional melt processing of glasses [6]. It involves the synthesis of a solution (sol), typically composed of metal-organic and metal salt precursors followed by the formation of a gel by chemical reactions (hydrolysis and condensation), and lastly thermal treatment for drying, organic removal, and oxide formation [7]. In sol-gel route, precursors are used to form and assemble nanoparticles into a gel at room temperature. Glass is formed after drying and heating this gel, which is a wet, organic, covalently bonded network. Lower fabrication temperature and the better control on composition and homogeneity are the main advantages of sol-gel over melt casting technique. Additionally, the most important difference between glasses produced by these methods is the presence of porosity with the sol-gel technique, which leads to an increase in surface area [2, 4, 5].

The synthesis of silicate based bioactive glasses by the sol–gel technique at low temperatures using metal alkoxides as precursors was shown by Li *et al*. [4]. After hydrolysis and poly-condensation reactions a gel is formed which subsequently is calcined at 600-700° C to form the glass. Similarly, fine powders (5 μm) of 45S5 (a Na_2O-containing composition) glass have been successfully synthesized using sol-gel technique in aqueous solution by Chen *et al*.[8] More recently, a new sol-gel route was developed by Pirayesh et al. [9] to produce silicate based 45S5 bioactive glass-ceramic powders. Based on their results, sol-gel derived 45S5 glass-ceramic and melt-cast amorphous 45S5 glass showed relatively similar HA formation rates. An alternative to 45S5 the so called 13-93 has been developed using melt-cast method and has been approved for in vivo use in Europe [10]. Based on 45S5, 13-93 has comparatively higher SiO_2 content and additional network modifiers such as K_2O and MgO. Furthermore, 13-93 bioactive glass exhibits better processing characteristics by viscous flow sintering enabling densification of glass scaffolds

without crystallization [3]. Despite its advantages, the sol-gel technique has not been yet applied to the production of 13-93 bioactive glass powders.

Different ions can be added to bioactive glasses, such as zinc, magnesium, zirconium, titanium, boron, strontium, copper and silver in order to improve the glass functionality and bioactivity [11-15]. Delben *et al*. [16] have developed sol–gel-derived bioactive glass doped with silver and reported that the Si–O–Si bond number increased with increasing silver concentration and this resulted in structural densification. It was also observed that quartz and metallic silver crystallization increased with the increase in silver content in bioactive glass while hydroxyapatite crystallization decreased. Previous studies revealed that addition of cerium and gallium may affect the bioactivity of silicate and borate based systems [17,18]. Both cerium oxide nanoparticles and gallium ions have gained considerable interest in biomedical field because of their potential therapeutic applications in metabolic bone, cancer and infectious diseases. However, sol-gel synthesis of 13-93 bioactive glass powders and effect of cerium and gallium ions on their glass forming ability and their in vitro response has not been studied yet to the best of our knowledge. Therefore, in this study it was intended to synthesize pure and Ce_2O_3 or Ga_2O_3 -doped 13-93 bioactive glass powders through sol-gel method and perform subsequent characterizations.

2. Materials and Methods

2.1. Powder Synthesis

For the synthesis of bioactive glasses, typical precursors used are tetraethyl orthosilicate (TEOS), triethyl phosphate (TEP), calcium nitrate tetrahydrate ($Ca(NO_3)_2.4\ H_2O$, potassium nitrate KNO_3, Magnesium nitrate hexahydrate ($Mg(NO_3)_2.6H_2O$), sodium nitrate $NaNO_3$, cerium(III) nitrate hexahydrate ($Ce(NO_3)_3{\cdot}6H_2O$) and gallium(III) nitrate hydrate ($Ga(NO_3)_3{\cdot}xH_2O$) (all from Sigma-Aldrich, USA). Table I show the composition of the bioactive glass powders synthesized in the study. For the preparation of the glass sols, initially 39.676 ml TEOS was added into 0.3 M HNO_3 aqueous solution at room temperature. The molar ratio of H_2O/TEOS was maintained at 15. The mixture was allowed to stir for at least 60 minutes for hydrolysis. Then each compound (1.90 ml TEP, 3.340 g $NaNO_3$, 16.538 g $Ca(NO_3)_2.4\ H_2O$, 6.317 g $Mg(NO_3)_2.6H_2O$, 5.230 g KNO_3) was added (in the sequence) only when the previous solution became clear and was stirred for 1 hour. Additionally, specified amount of $Ce(NO_3)_3{\cdot}6H_2O$ or $Ga(NO_3)_3{\cdot}xH_2O$ (depending on the substitution level; 1, 3 or 5 wt%) were added to the above solution to prepare cerium and gallium-containing 13-93 glass sol. The resulting transparent solution was stirred overnight for homogenization in a closed bottle and then stored at room temperature. In this solution gelation occurred after 3 days at 25 ºC. During sol formation, the TEOS undergoes a hydrolysis reaction, creating the silanol groups. The hydrated silica interacts in a condensation reaction forming Si-O-Si bonds. The gel was aged for 48 hours at 60 ºC and then dried at 120 ºC for 24 hours. During ageing process the aqueous gel continues to crosslink the silicate structure, resulting in the formation of a glass network. The dried sample was ground using an agate mortar and then a heat treatment at 625 C ºC for 4 hours was applied to remove the nitrates in the structure. Heat treatment regime was based on a previous study on the preparation 13-93 nanofibers [19]. After calcination step powders were ground for 5 minutes using a vibratory disc mill (Retsch RS 200, Düsseldorf, Germany) at 1000 rpm.

Table I. Composition of the glasses (in wt%) prepared in this work.

Glass	SiO_2	CaO	Na_2O	K_2O	MgO	P_2O_5	Ce_2O_3	Ga_2O_3
13-93 (B0)	53	20	6	12	5	4	-	-
1Ce-B0	52	20	6	12	5	4	1	-
3Ce-B0	50	20	6	12	5	4	3	-
5Ce-B0	48	20	6	12	5	4	5	-
1Ga-B0	52	20	6	12	5	4	-	1
3Ga-B0	50	20	6	12	5	4		3
5Ga-B0	48	20	6	12	5	4	-	5

2.2. Characterizations

The microstructure of the fabricated bioactive glass powders were examined using SEM (Philips XL-30S FEG, Netherlands) at an accelerating voltage of 5 kV and a working distance of 10 mm. X-ray diffraction, XRD (Philips X'Pert Pro, Netherlands) was used to determine the presence of any crystalline phase formation in the as-prepared powders; XRD was performed using Cu Kα radiation at a scanning rate of 0.01°/min in the range 3–90° 2θ. Fourier transform infrared spectroscopy (FTIR-ATR, Agilent Cary 660,Santa Clara, United States) was utilized to analyse the identification of the glass forming structural units in the powders. Particle size measurements were performed using a laser diffraction particle size analyser (Malvern, Mastersizer 3000, Worcestershire, UK). For the measurements dilute

aqueous suspension of bioactive glass powders were prepared and ultrasonification was applied for 7 minutes for homogenization. The devices use dynamic light scattering technique and data is analysed to calculate the size of the particles based on Mie and Fraunhofer scattering theories.

2.2.1. In vitro Bioactivity

The degradation and bioactivity of the scaffolds was investigated in vitro in a simulated body fluid (SBF) under static conditions. SBF was prepared in compliance with the protocol of Kokubo *et al.* [20], by dissolving reagent-grade chemicals of NaCl, $NaHCO_3$, KCl, $K_2HPO_4{\bullet}3H_2O$, $MgCl_2{\bullet}6H_2O$, $CaCl_2$ and Na_2SO_4 (Sigma Aldrich, Germany) in deionized water and buffering at a pH of 7.40 with tris(hydroxymethyl)aminomethane ($(CH_2OH)_3CNH_2$) and 1 M hydrochloric acid (Fisher Scientific Inc., USA). Ratios of 1 g of powder to 100 ml to 1000 ml of SBF was used in the conversion experiments. Each glass composition was immersed in a polyethylene bottle containing the SBF solution, and kept for varying time periods, without shaking, in an incubator at 37 °C. After removal from SBF powders were rinsed with deionized water and dried at 60 °C prior to characterizations. Ultra-pure water with a resistivity of 18 MΩ-cm was used through the experiments. SEM and FTIR-ATR was used to characterize HA-like layer formed on the surfaces of the glass powders using conditions described previously. For comparison purposes FTIR analysis of a commercial un-treated HA powder was performed under the same conditions.

2.2.2 Mechanical Properties

Vickers hardness testing was performed to measure the surface hardness of the substituted bioactive glass samples. Hardness measurements were conducted using a Emco-Test DuraVision hardness tester (Kuchl, Austria). Prior to measurements the surface of the die pressed disc- shaped samples (sintered at 690 ºC) were ground with SiC grinding papers of 600 through 1200 grit size.. Indentations were conducted using a Vickers diamond pyramid at 1000, 3000 and 5000 g load for 15 seconds. Five different measurements were carried out on each sample and the results were averaged. The crack formation on the samples was analyzed using an optical microscope (Nikon Eclipse LV 100, Amsterdam, Netherlands) using Clemex Software (Canada).

The compressive strength of the scaffolds was measured using a mechanical testing device (Shimadzu Autograph, AG-IS, Japan) at a crosshead speed of 0.5 mm/min. Three samples were measured for each group of scaffold and the average strength was determined.

3. Results and Discussion

Figure 1 shows the SEM micrographs of the sol-gel derived cerium and gallium (5w%) containing 13-93 glass powders after calcination at 625 ºC. Accordingly, particles have an irregular morphology and wide distribution of sizes. Size of the cerium and gallium containing powders were relatively higher compared to that of bare 13-93 glass powders. Additionally, formation of a second phase material was observed on the surface of the 5Ce-B0 powders. Particle size of the synthesized powders was tabulated in Table II. The measured values again indicated that powders show relatively wide range of diameters. Especially, cerium-containing samples have much higher median diameter values compared to other compositions. Besides, an increase was observed in particle size as the cerium concentration was increased.

XRD diagrams of the bioactive glass powders prepared in the study (after calcination) are given in Figure 2. Based on the diffraction patterns crystallization was not observed in most of the compositions. Substitution of gallium even at highest concentration did not cause any crystalline phase formation in the glass network. Only for the cerium-containing powders starting from 3%Ce some peaks of ceria appeared. XRD patterns of 3Ce-B0 and 5Ce-B0 contained four major peaks assigned to the (1 1 1), (2 0 0), (2 2 0), (3 1 1) planes of ceria (CeO_2) PDF # 81-0792 [21]. The glass composition 1Ce-B0 showed no diffraction peaks for ceria and this may be attributed to the low amount of ceria, which was below the detection range of the XRD instrument. Results are in good agreement with the previous findings of Goh *et al*.[21] on ceria containing bioactive glasses. On the other hand, results also revealed it is possible to produce amorphous 13-93 glass powders by sol-gel process developed in the study. Calcination at 625 ºC was sufficient to remove the all the nitrates in the structure and low enough to avoid crystallization. However, 13-93 powders calcined at 610 ºC showed the diffraction peaks of sodium nitrate in the structure (Fig.2-a).

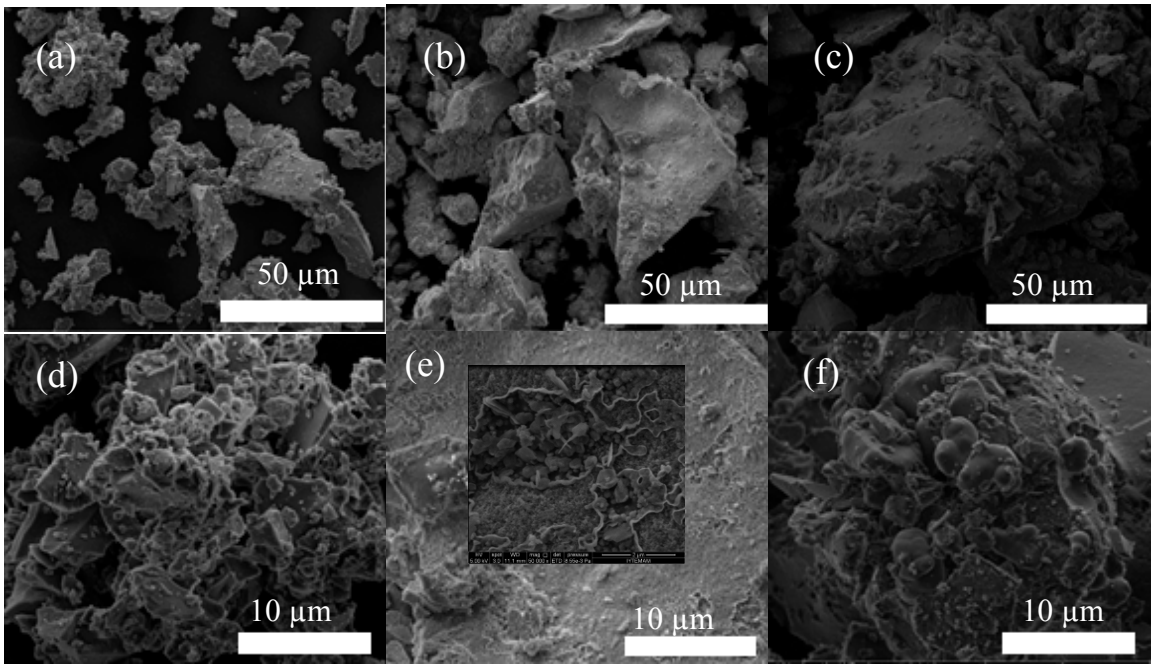

Figure 1. SEM micrographs of the (a),(d) bare 13-93; (b),(e) cerium (5Ce-B0) and (c), (f) gallium-containing (5Ga-B0) bioactive glass powders after calcination at 625 ˚C.

Table II. Particle size analysis results of the sol-derived bioactive glass powders.

Glass Composition	D_{10} (µm)	D_{50} (µm)	D_{90} (µm)
13-93 (B0)	6.65	68.9	104
1Ce-B0	9.93	75.8	175
3Ce-B0	11.0	137	189
5Ce-B0	13.7	145	221
1Ga-B0	10.0	65.9	132
3Ga-B0	11.3	62.0	151
5Ga-B0	10.7	51.7	138

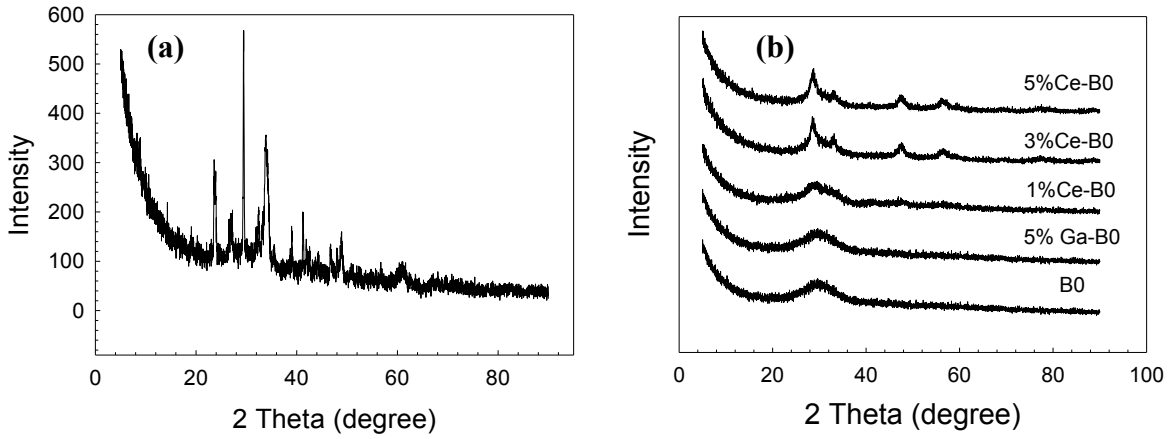

Figure 2. XRD diagrams of the sol-gel derived (a) 13-93 glass composition after calcination at 610 ºC, (b) cerium and gallium- containing bioactive glass powders after calcination at 625 ºC.

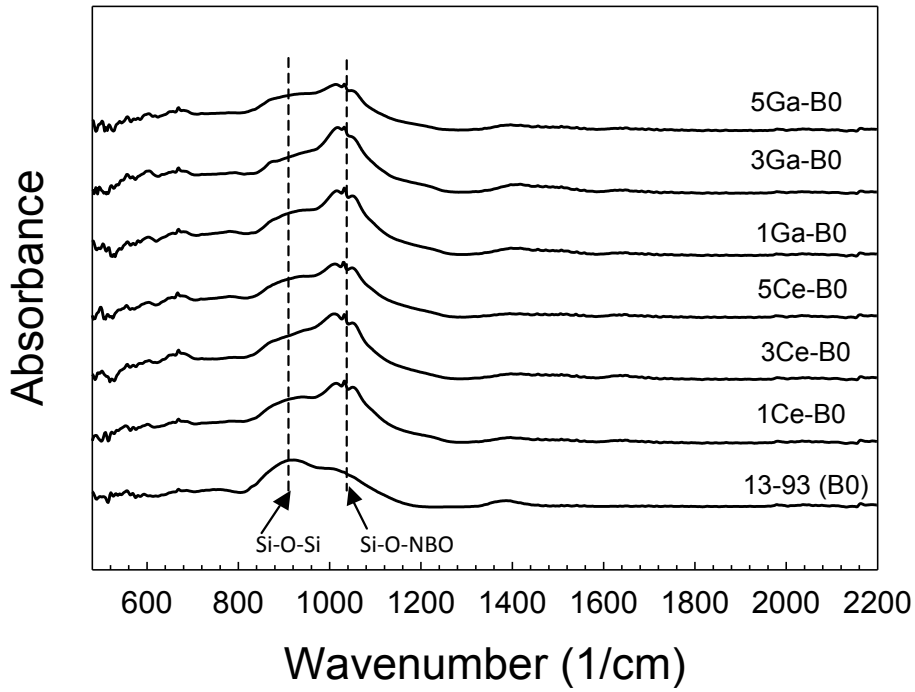

Figure 3. FTIR spectra of the sol-gel derived as-prepared bioactive glass powders containing cerium and gallium at different substitution levels.

FTIR spectrum of the as-prepared powders is shown in Fig.3. The primary resonances in the spectrum for the all of the powders synthesized in the study consisted of the vibrational modes of the Si-O-Si such as stretching vibration band in the range 950-1050 cm^{-1}. The resonances in the range of 850-950 cm^{-1} corresponded to Si-O-2NBO (non-bridging oxygen) vibrational modes associated with the Ca, Na, Mg and K ions in the glass network [22]. By the introduction of the cerium and gallium ions to the network structure an increase was observed in the intensity of the Si-O-2NBO band and a decrease was noticed for the Si-O-Si stretching vibration band. In network-modified

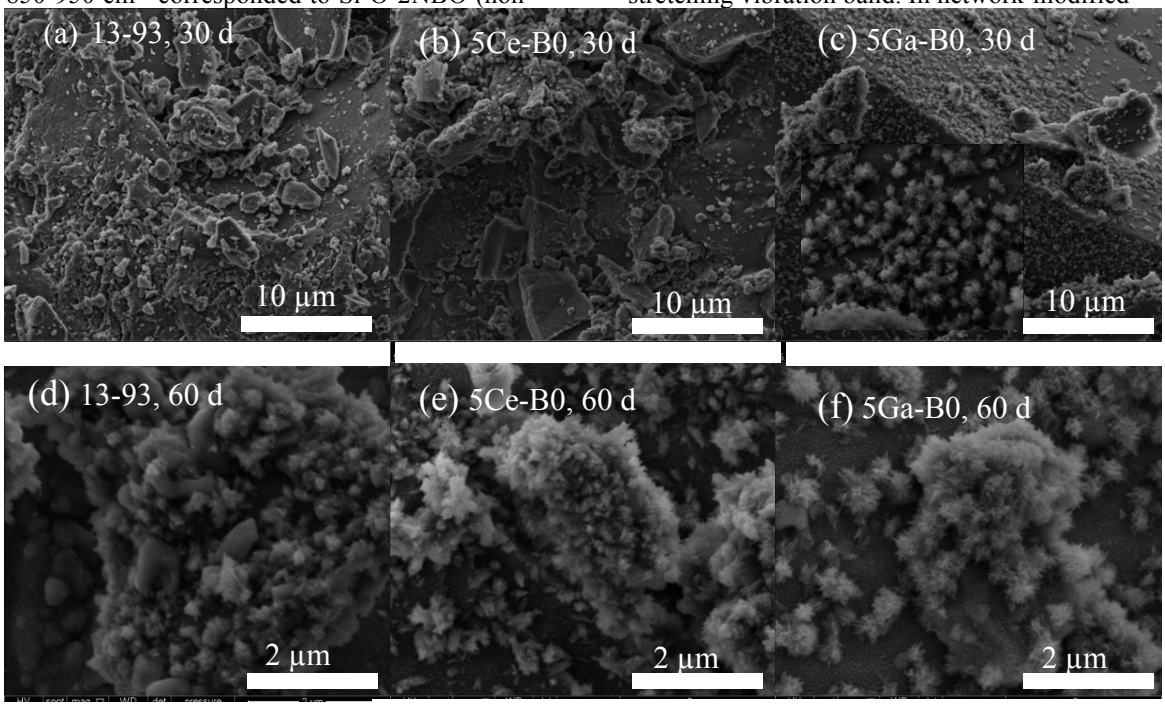

Figure 4. SEM micrographs of the 13-93, 5Ce-B0 and 5Ga-B0 bioactive glass powders treated in SBF (100 ml/g) for (a),(b),(c) 30 days and (d),(e),(f) 60 days.

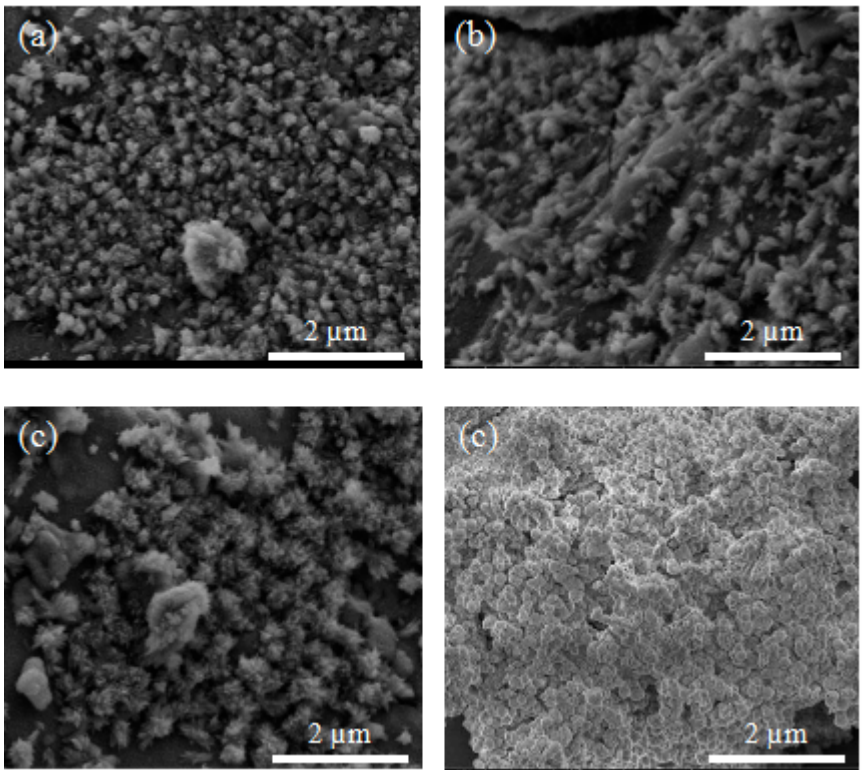

Figure 5. SEM micrographs of the (a) 13-93, (b) 5Ce-B0 and (c) 5Ga-B0 bioactive glass powders treated in SBF (1000 ml/g) for 30 days; (d) 13-93 treated in SBF (500 ml/g) for 30 days.

silicate glasses, network of SiO_4 tetrahedra is disrupted by modifying cations which create non-bridging oxygens [23]. When a network modifier is added to SiO_2 glass a number of Si-O bonds are broken. The added oxygen saturates the unsatisfied bond of one Si and the two $Si\text{-}O^-$ bonds are created. The negative charge of the oxygen ion is compensated by the modifier ion [24]. The presence of non-bridging oxygens lowers the relative number of strong bonds in the material and disrupts the network, decreasing the viscosity of the melt and lowering the melting temperature. A previous study [17] on mesoporous bioactive glasses with the composition (80 x)% SiO_2–15% CaO–5% P_2O_5 (in mol.%) showed that the glass network connectivity of un-substituted glass reduced upon the addition of Ce ions, which thus acts mainly as a network modifier, while gallium and zinc ions behave as intermediate ions. However, in the current study Ce and Ga ions presumably acted as a modifier ion in the 13-93 silica glass network. Additionally, crystalline CeO_2 formation in cerium-containing samples (at 3 and 5%) was not detected in FTIR spectra. The FTIR spectrum of the ceria exhibits strong broad band below 700 cm^{-1} which is due to the δ (Ce–O–C) mode [21]. However, X-Ray diffraction patterns of these samples contain major peaks of the ceria. In vitro bioactivity and the HA layer formation on the prepared bioactive glass powders were investigated in simulated body fluid at 37 ºC as a function of immersion time and the SBF- glass powder ratio. Figure 4 show the SEM micrographs of the bioactive glass powders after soaking in SBF (100 ml SBF/1 gr glass powder) for 30 and 60 days. Accordingly, the formation of a second phase on the powders treated in SBF for 30 days is barely observed. Only in the case of 5Ga-B0 powder composition a second phase material presumably an amorphous calcium phosphate is detected on the surface. On the other hand, after 60 days of immersion for all the compositions tested in the study some calcium phosphate precipitates were detected. Newly formed material has a needle shape and covered partly of the glass surface as aggregates. A significant difference was not observed on the shape and the morphology of this material as a function glass composition and doping element concentration.

SEM micrographs of the samples treated in SBF (1000 ml SBF / 1 g glass powder) for 30 days are shown in Figure 5. Results revealed that the surface of the bare 13-93 and the therapeutic element (Ce and Ga)-containing samples was covered with the calcium phosphate based material. Additionally, for the bare sample treated in SBF at higher glass powder ratio (500 ml SBF/ 1 g glass) formation of a similar type of material was again observed after 30 days of immersion (Fig.5-d).

FTIR spectra of the bioactive glass powders treated in SBF at 100 ml/g and 1000 ml/g are shown in Fig. 6 and Fig. 7, respectively. In Figure 6, the main absorption bands which represent amorphous glass are Si-O stretching at ~920 cm^{-1} and 1040 cm^{-1}. The

two P-O pending peaks at 560 and ~600 cm^{-1} are the main peaks for characterizing the crystalline HA [9,22,25]. FTIR spectrum of commercial hydroxyapatite powder is shown in Fig. 8 for comparison purposes. These peaks are barely observed in samples treated in SBF (100 ml/g) for 30 days. On the other hand, higher intensity in P-O pending peaks in the samples immersed in SBF with 1000 ml/g for 30 days. This means that higher HA formation was observed in samples immersed in SBF at lower glass concentrations. Additionally, in the spectrum the peak at 880 cm^{-1} is attributed to the C-O stretching [22]. In Fig. 7 low intensity C-O stretching peak was present in Ce and Ga-containing samples. In the spectrum the peak at 1100 cm^{-1} corresponds to P-O bonds which represent the HA. However, P-O stretching bond at 1100 cm^{-1} superimposed on the Si-O stretching bonds. Therefore, in the study only the peaks at 560 and ~600 cm^{-1} were considered for the evaluation of HA formation.

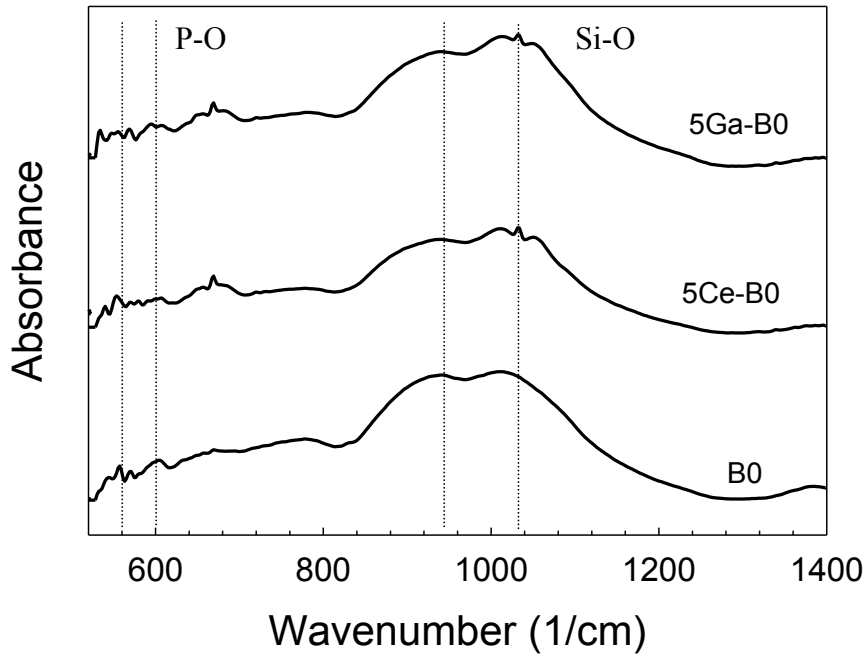

Figure 6. FTIR spectra of the bioactive glass powders treated in SBF (100 ml/g) for 30 days.

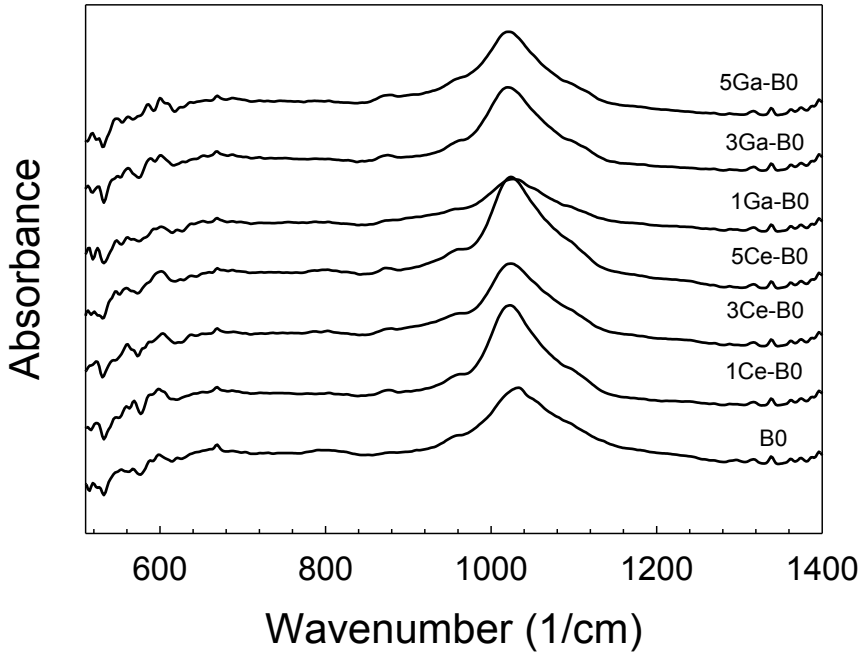

Figure 7. FTIR spectra of the bioactive glass powders treated in SBF (1000 ml/g) for 30 days.

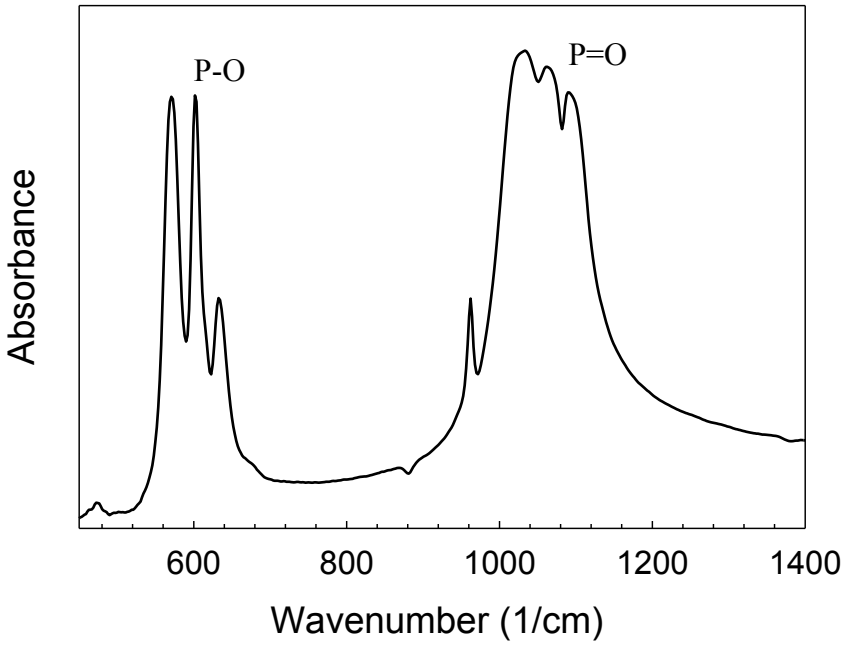

Figure 8. FTIR spectrum of the synthetic HA powder.

Vickers Hardness of the cerium and gallium-containing glass specimens prepared in the study was measured to investigate the effect of therapeutic ions utilized on the mechanical performance of the substituted 13-93 glass. Table III and Table IV show the hardness values (H_v) of the gallium and cerium containing glass pellets, respectively. Accordingly, a slight decrease was observed in hardness values of the gallium-containing glass discs as the gallium concentration was increased. The Vickers hardness number of the 1Ga-B0 glass composition was measured to be 419± 18.53 (at 3000 g) whereas it decreased to 382± 19.81 for the 5Ga-B0 glass under the same conditions.

Table III. Vickers hardness numbers of gallium-containing bioactive glass samples.

Glass composition	1Ga-B0	3Ga-B0	5Ga-B0
H_v, (at 1000 g)	424± 35.15	420± 19.86	395± 21.42
H_v, (at 3000 g)	419± 18.53	416± 14.89	382± 19.81
H_v, (at 5000 g)	416± 23.62	411± 30.09	381± 23.12

Table IV. Vickers hardness numbers of cerium-containing bioactive glass samples.

Glass composition	1Ce-B0	3Ce-B0	5Ce-B0
H_v, (at 3000 g)	420± 25.17	432± 15.36	445± 21.32

The Vickers hardness number of the bare 13-93 glass was measured to be 421± 12.43 at the same indentation load. Results also revealed a slight variation in hardness values of Ga-containing samples as the indentation load was increased. Similarly, hardness values of the cerium-containing bioactive glass specimens are tabulated in Table IV. Higher values were obtained for cerium containing (3%Ce and 5%Ce) samples compared to the gallium-substituted glass. This may be attributed to the CeO_2 crystal formation on the surface of the samples during heat treatment. Figure 9, show the variation in Vickers Hardness numbers (in GPa) of the metal ion substituted glass specimens.

To convert the Vickers hardness numbers the force applied converted from kgf to newton and the area converted from mm^2 to m^2 to give results in Pascal using the formula equation 1:

$$H_{v=}\frac{2F\ Sin\ \frac{136°}{2}}{d^2} \quad (1)$$

The optical microscope images of the surface of bare 13-93 and the 5Ga-B0 glass samples after indentation test is demonstrated in Figure 10. Some surface irregularities formed on the glass after polishing step. Crack formation was observed on the corners of diagonals created by the indenter (at 3000 g load). The total crack length (372.7 µm, summation of lengths of all of the cracks) was higher for the sample 5Ga-B0 compared to the total crack length for the bare 13-93 sample (501.9 µm) and cracks were coming from the corners of the indentation. The growth of a surface flaw depends on the properties of the flaw and the glass, the stress history that the flaw is exposed to and the relationship between crack velocity and stress intensity factor [26, 27]. The decrease observed in hardness values and the increase in total crack length in Ga-containing samples may be attributed to the acting of gallium as a modifier ion as it was discussed in previous section. By the introduction of the gallium to the structure SiO_4 tetrahedra is presumably disrupted which create non-bridging oxygens. The presence of non-bridging oxygens lowers the relative number of strong bonds in the material and disrupts the network [28]. On the other hand, in the case of cerium substitution, the crystallization observed in glass powders and disc shape specimens after calcination at 625 ºC and sintering at 690 ºC, respectively. This may be reason of the observed increase in hardness values of the cerium containing glass samples.

Compression strength of the disc shaped glass scaffolds was also measured in the study and the results are tabulated in Table V. Accordingly, compression strength of the Ga-containing samples was lower than the bare 13-93 glass. On the other hand, higher strength values were obtained in Ce-containing samples starting from 3%Ce. Compression strength of the 5Ce-B0 sample was measured to be 345.45± 35 MPa whereas it was 119.45± 15 MPa for the 5Ga-B0 glass. The difference obtained in compression strength values was again attributed to the network disruption effect of gallium ions in silica tetrahedra which causes a weakly bonded structure and the CeO_2 crystal formation which may improve the strength of the network.

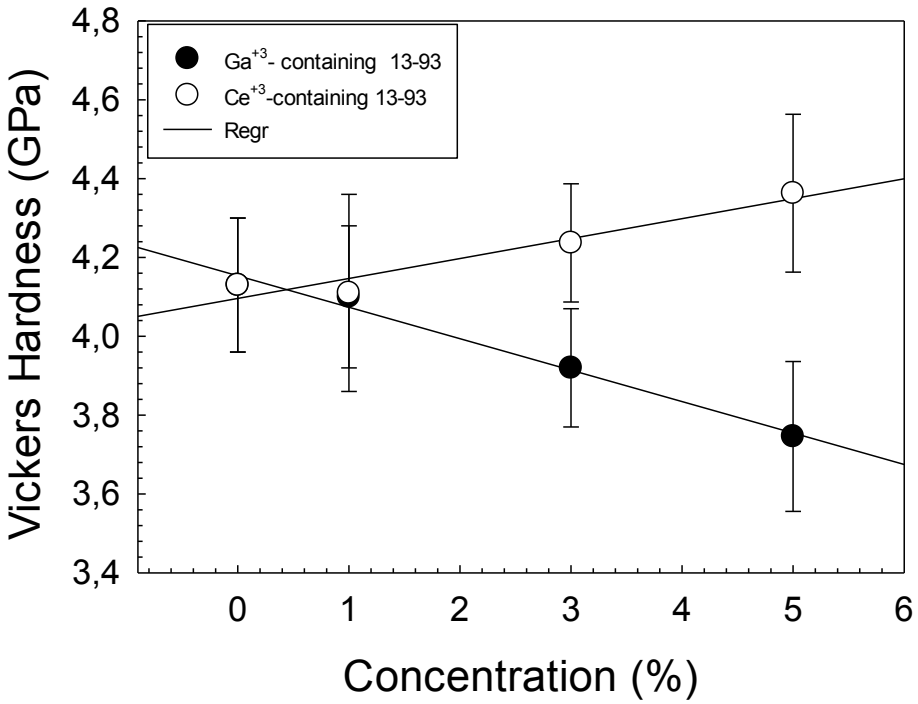

Figure 9. Graph showing the Vickers hardness values (GPa) of bioactive glass specimens as a function of cerium and gallium substitution level.

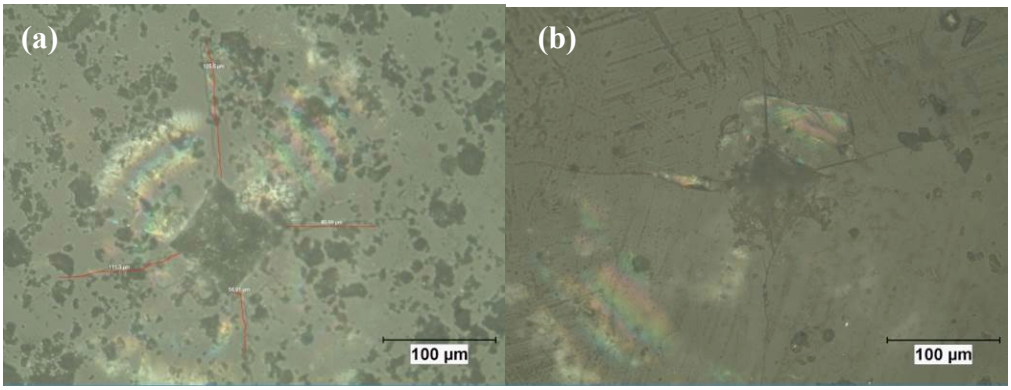

Figure 10. Optical microscope images showing the surface of the (a) 13-93 and (b) 5Ga-B0, disc shape bioactive glass samples after indentation at 3000 g load. Magnifications X 20.

Table V. Compression strength values of the bioactive glass samples prepared in the study.

Bioactive glass composition	Compression Strength (N/mm^2)
B0	197.24± 15
1Ce-B0	186.06± 21
3Ce-B0	215.01± 17
5Ce-B0	345.45± 35
1Ga-B0	131.43± 22
3Ga-B0	128.13± 12
5Ga-B0	119.45± 15

4. Conclusions

Cerium and gallium-containing (up to 5w%) 13-93 based bioactive glass powders were successfully fabricated using sol-gel process. Sol-derived powders kept their amorphous nature after a heat treatment at 625 °C and any crystallization was not observed except for 3Ce-B0 and 5Ce-B0 glass compositions. Fabricated powders showed a bioactive response in simulated body fluid. A crystalline Ca-P layer, as indicated by the divided P-O bending vibration band between 550 and 610 cm^{-1}, formed for all samples immersed in SBF (1 g glass/1000 ml SBF) for 30 days. A decrease in hardness and compression strength values were obtained in gallium-containing samples and it was attributed to the network modifier effect of gallium ions. On the other the observed increase in hardness and strength values of the cerium substituted glasses was presumably due to the CeO_2 crystal formation during heat treatment. Results revealed that sol-gel derived silicate based bioactive glasses containing therapeutic elements (Ce and Ga) could be utilized in tissue engineering applications without significant loss in HA forming ability.

Acknowledgements

The financial support for this research was provided by the Scientific and Technical Research Council of Turkey (TUBITAK), 1001 grant program for scientific and technological research projects; grant no: 111M766.

References

1. **L.L.Hench**, Chronology of Bioactive Glass Development and Clinical Applications, New *Journal of Glass and Ceramics*, 3, 67-73.
2. **A. Polini, H. Bai, A.P. Tomsia**, Dental applications of nanostructured bioactive glass and its composites. *Wiley interdisciplinary reviews Nanomedicine and nanobiotechnology*. 5(4):399-410.
3. **M.N.Rahaman, D.E.Day, B.S. Bal, Q.Fu, S.B. Jung, L.F. Bonewald**, Bioactive glass in tissue engineering, *Acta Biomater*., 7: 2355-73.
4. **R.Li, A.E. Clark, L.L. Hench**, An investigation of bioactive glass powders by sol-gel processing, *J Appl Biomater*. 2:231–239.
5. **P. Sepulveda, J.R. Jones, L.L. Hench**, Characterization of melt-derived 45S5 and sol-gel-derived 58S bioactive glasses, *J Biomed Mater Res*., 58:734–740.
6. **J. Zhong, D.C. Greenspan**, Processing and Properties of Sol–Gel Bioactive Glasses, *J Biomed Mater Res :Appl Biomater*. 53: 694–701.
7. **M.N.Rahaman**, Ceramic Processing and Sintering, Chapter 5, pages 201-261, Marcel Dekker, USA.
8. **Q-Z. Chen, Y. Li, L-Y. Jin, J.M.W. Quinn, P.A. Komesaroff**, A new sol-gel process for producing Na_2O containing bioactive glass ceramics, *Acta Biomater.*, 6, 4143-4153.
9. **H. Pirayesh, J.A. Nychka**, Sol-Gel synthesis of bioactive glass-ceramic 45S5 and its in

vitro dissolution and mineralization behavior, *J.Am.Ceram.Soc.,* 1-8.

10. **M. Brink, T. Turunen, R-P. Happonen, A. Yli-Urpo**, Compositional dependence of bioactivity of glasses in the system Na_2O-K_2O-MgO-CaO-B_2O_3-P_2O_5-SiO_2, *J. Biomed. Mater. Res.*, 37:114-121.
11. **W.C.A.Vrouwenvelder, C.G. Groot, K. Degroot**, Better histology and biochemistry for osteoblasts cultured on titanium doped bioactive glass — Bioglass 45S5 compared with iron-containing, titanium-containing, fluorine containing and boron-containing bioactive glasses, *Biomaterials 1*5, 97–106.
12. **S.Haimi, G. Gorianc, L. Moimas, B. Lindroos, H. Huhtala, S. Räty, H. Kuokkanen, G.K. Sándor, C.Schmid, S. Miettinen, R. Suuronen**, Characterization of zinc-releasing three Dimensional bioactive glass scaffolds and their effect on human adipose stem cell proliferation and osteogenic differentiation, *Acta Biomater.*, Vol. 5, No. 8, 3122-3131.
13. **V. Aina, G. Lusvardi, G. Malavasi, L. Menabue, C. Morterra**, Fluoride-containing bioactive glasses: surface reactivity in simulated body fluids, *Acta Biomater.* 5, 3548–3562.
14. **E.Gentleman, Y.C. Fredholm, G. Jell, N. Lotfibakhshaiesh, M.D. O'Donnell, R.G. Hill, M.M. Stevens**, The effects of strontium-substituted bioactive glasses on osteoblasts and osteoclasts in vitro, *Biomaterials*, 31(14): 3949-3956.
15. **S.J. Watts, R.G. Hill, M.D. O'Donnell, R.V. Law**, Influence of magnesia on the structure and properties of bioactive glasses, *J. Non-Cryst. Solids*, 356:517-24.
16. **J.R.J. Delben, O.M.Pimentel, M.B. Coelho, P.D.Candelorio, L.N. Furini, F.A. Santos, F.S. Vicente, A.A.S.T. Delben**, Synthesis and thermal properties of nanoparticles of bioactive glasses containing silver. *J Therm Anal Calorim*. 97:433–436.
17. **A.J. Salinas, S. Shruti, G. Malavasi, L. Menabue, M. Vallet-Regi**, Substitution of cerium, gallium and zinc in ordered mesoporous bioactive glasses. *Acta Biomater*. 7, 3452–8.
18. **A.M.Deliormanlı**, Synthesis and characterization of cerium- and gallium-containing borate bioactive glass scaffolds for bone tissue engineering. *J. Mater. Sci. Mater. Med*. 26(2):67.
19. **A.M. Deliormanlı**, Preparation, in vitro mineralization and osteoblast cell response of electrospun 13-93 bioactive glass nanofibers. *Mater. Sci. Eng. C., 53:262-71*.
20. **T. Kokubo, H. Kushitani, S. Saka, T. Kitsugi, T. Yamamuro**, Solutions able to reproduce in vivo surface-structure changes in bioactive glass-ceramic A-W, *J. Biomed. Mater. Res.,* 24:721-734.
21. **Y-F. Goh, A.Z. Alshemary, M. Akram, M.R.F. Kadir, R. Hussain**, In vitro characterization of antibacterial bioactive glass containing ceria", *Ceram. Int.*, 40 (1), 729-737.
22. **X. Liu, M.N. Rahaman, D.E. Day**, Conversion of melt-derived microfibrous borate (13-93B3) and silicate (45S5) bioactive glass in a simulated body fluid, *J. Mater. Sci. Mater. Med*., 24:583-95.
23. **I. Farnan, P.J. Grandinetti, J.H. Baltisberger, J.F. Stebbins, U. Werner, M.A. Eastman, A. Pines**, Quantification of the disorder in network-modified silicate glasse, *Nature*, 2;358(6381):31-5.
24. **C.B. Carter and M.G. Norton**, Ceramic Materials: Science and Engineering, Chapter 7: complex crystal and glass structures, Springer Science & Business Media, 766.
25. **H.H.Lu, Pollack SR, P. Ducheyne**, 45S5 Bioactive glass surface charge variations and the formation of a surface calcium phosphate layer in a solution containing fibronectin, *J. Biomed. Mater. Res*., 54: 454-461.
26. **M. Overend, S.D. Gaetano, M. Haldimann**, Diagnostic Interpretation of Glass Failure, *Structural Engineering International*, 2, 151.
27. **S. Roy, B. Basu**, Hardness properties and microscopic investigation of crack–crystal interaction in SiO2–MgO–Al2O3–K2O–B2O3–F glass ceramic system, *J.Mater. Sci: Mater. Med*., 21, Issue 1, 109-122.
28. **R.A. Martin, S. Yue, J.V. Hanna, P.D. Lee, R.J. Newport, M.E. Smith, J.R. Jones**, Characterizing the hierarchical structures of bioactive sol–gel silicate glass and hybrid scaffolds for bone regeneration, *Phil. Trans. R. Soc. A,* 370, 1422–1443.